Microstructure and Mechanical Properties of Nano-Size Zirconium Carbide Dispersion Strengthened Tungsten Alloys Fabricated by Spark Plasma Sintering Method

2015 Plasma Sci. Technol. 17 1066

(http://iopscience.iop.org/1009-0630/17/12/1066)

Microstructure and Mechanical Properties of Nano-Size Zirconium Carbide Dispersion Strengthened Tungsten Alloys Fabricated by Spark Plasma Sintering Method*

XIE Zhuoming (谢卓明)[1,2], LIU Rui (刘瑞)[1], FANG Qianfeng (方前锋)[1,2], ZHANG Tao (张涛)[1], JIANG Yan (蒋燕)[1], WANG Xianping (王先平)[1], LIU Changsong (刘长松)[1]

[1]Key Laboratory of Materials Physics, Institute of Solid State Physics, Chinese Academy of Sciences, Hefei 230031, China
[2]University of Science and Technology of China, Hefei 230026, China

Abstract W-(0.2, 0.5, 1.0)wt% ZrC alloys with a relative density above 97.5% were fabricated through the spark plasma sintering (SPS) method. The grain size of W-1.0wt% ZrC is about 2.7 μm, smaller than that of pure W and W-(0.2, 0.5)wt% ZrC. The results indicated that the W-ZrC alloys exhibit higher hardness at room temperature, higher tensile strength at high temperature, and a lower ductile to brittle transition temperature (DBTT) than pure W. The tensile strength and total elongation of W-0.5wt% ZrC alloy at 700 °C is 535 MPa and 24.8%, which are respectively 59% and 114% higher than those of pure W (337 MPa, 11.6%). The DBTT of W-(0.2, 0.5, 1.0)wt% ZrC materials is in the range of 500 °C-600 °C, which is about 100 °C lower than that of pure W. Based on microstructure analysis, the improved mechanical properties of the W-ZrC alloys were suggested to originate from the enhanced grain boundary cohesion by ZrC capturing the impurity oxygen in tungsten and nano-size ZrC dispersion strengthening.

Keywords: tungsten, zirconium carbide, mechanical property, dispersion strengthening

PACS: *28.52.Fa, 81.05.Bx, 81.20.Ev, 62.20.fk*

DOI: 10.1088/1009-0630/17/12/15

(Some figures may appear in colour only in the online journal)

1 Introduction

Tungsten has been extensively used as the solid target in a spallation neutron source and is considered as the candidate of first wall materials in future fusion reactors because of its excellent properties, such as large atomic mass, high melting temperature, high thermal resistance, low tritium retention, and low physical sputtering yield [1−3]. However, tungsten undergoes serious embrittlement in several regimes, including room-temperature brittleness, recrystallization brittleness and irradiation induced brittleness [3−5]. Meanwhile, experiments indicate that impurities such as oxygen, phosphorous and nitrogen, which segregate in the grain boundaries (GBs), are thought to have a significant effect on the fracture toughness of tungsten [6−8]. As a result, polycrystalline W has a high ductile-to-brittle transition temperature (DBTT) of about 800 °C. Therefore, eliminating the effect of such detrimental impurities on GBs and enhancing the coherent strengthening of GBs are of considerable significance for improving the performance of W based materials.

Using vacuum and zone melting can reduce impurity concentration and lower the DBTT to about 200 °C [9], but pure W has low strength (especially at high-temperature) and undergoes recrystallization at relatively low temperature (∼1200 °C) which further reduces the fracture toughness [10]. Increasing the density of GBs by severe plastic deformation could decrease the average concentration of impurities at GBs, and thus improves the toughness of W [11], but the large volume fraction of GBs would also lead to an inherent instability especially at high temperatures [12]. Dispersing small amounts of carbide or oxide fine particles with high thermodynamic stability, such as TiC, ZrC, La_2O_3 and Y_2O_3, into tungsten, is very effective in inhibiting the grain growth and stabilizing the microstructure at high temperature [4,12,13]. The dispersed carbides or oxides could greatly improve the high temperature strength, increase the recrystallization temperature and enhance the creep resistance of tungsten [4,14,15]. Besides, the large volume fraction of GBs regions and particle-matrix interfacial regions in these materials can also provide sinks for irradiation induced point defects and hence improve the irradiation resistance [5,16,17]. For example, an ultrafine-

*supported by the Innovation Program of Chinese Academy of Sciences (No. KJCX2-YW-N35), the National Magnetic Confinement Fusion Science Program of China (No. 2011GB108004), National Natural Science Foundation of China (Nos. 51301164, 11075177, 11274305), and Anhui Provincial Natural Science Foundation of China (No. 1408085QE77)

grained W-TiC alloy showed high fracture strength of about 2 GPa at room-temperature, super-plasticity at 1400 °C-1700 °C and superior resistance to neutron irradiation [4].

Among the strengthening phases in tungsten alloys, ZrC has a very high hardness, and its melting temperature is as high as 3540 °C, much higher than TiC (3160 °C), La_2O_3 (2215 °C) and Y_2O_3 (2690 °C). The high hardness and melting temperature make ZrC very attractive in strengthening the high-temperature properties of tungsten. Besides, ZrC can react with oxygen at relatively low temperatures (∼600 °C) under a low oxygen pressure [18]. This may reduce the influence of oxygen on GBs of tungsten, and thus improve the cohesion of GBs. To illustrate this point, W-(0.2, 0.5, 1.0)wt% ZrC alloys are fabricated through the spark plasma sintering (SPS) method in this work. The effects of the different ratios of ZrC addition on the consolidation behavior, microstructure, and mechanical properties of tungsten samples are investigated.

2 Experimental details

W-(0.2, 0.5, 1.0)wt% ZrC samples were fabricated through a powder metallurgy method. Pure W (particle size of 400-600 nm, purity>99.9%, chemical content listed in Table 1, purchased from Xiamen Tungsten Co., LTD) and nano-size ZrC (average particle size of 50 nm, purity>99%, purchased from Aladdin reagent Co., LTD) powders were used as starting materials. Powders were ball milled in a planetary ball mill for 4 h in argon atmosphere with a powder-to-ball weight ratio of 1:8 and a rotation speed of 240 rpm. Tungsten carbide balls (diameters between 6 mm and 10 mm, purchased from Nanjing Nanda Instrument Co., LTD) and mortars were used to minimize the possible impurity contamination.

The consolidation of the samples was carried out in an SPS system (furnace SE-607, FCT Group, Germany). The pressure and temperature profile of the sintering program in this study was described in an earlier work [19]. The as-prepared powders were loaded into a graphite mold and then heated to 1800 °C by a pulse current (1000-5000 A) and held for 2 min under a uniaxial pressure of 47.7 MPa. The heating rates at temperatures below and above 1300 °C were 100 °C/min and 50 °C/min, respectively. The cooling rate was 100 °C/min. All samples were spark-plasma-sintered (SPSed) following the same sintering program. The size of the SPSed samples was about 2.0 mm in thickness and 20 mm in diameter. During SPSing progress, a 50 μm thick WC layer was formed on the sample surface due to the reaction between tungsten and carbon from graphite molds, which was removed by Wire cut Electrical Discharge Machining in our laboratory. The rest samples were polished with 800, 1000, 1500, 2000 mesh SiC paper and a nylon polishing cloth for further tests.

The density of SPSed samples was determined by Archimedes' principle. The theoretical density of the W-(0-1.0)wt% ZrC composites was calculated from the fraction and theoretical density of each components. The theoretical densities of tungsten and zirconium carbide were taken as 19.25 g/cm^3 and 6.73 g/cm^3, respectively.

Polished samples were subjected to Vickers microhardness testing at room temperature with a load of 100 g and a dwell time of 10 s. For tensile testing, all of the SPSed samples were cut into dog-bone-shaped samples (with a cross-section of 1.5×0.75 mm^2 and a working length of 5 mm) and polished. Five tensile tests were carried out for each sample at various temperatures from 500 °C to 700 °C, using an Instron-5967 machine at a constant speed of 0.06 mm/min. The elongations were determined by measuring the length of fractured samples by using a vernier caliper.

The fracture surfaces of samples were characterized by a field-emission scanning electron microscope (FE-SEMSirion200, FEI). The average tungsten grain size was obtained from measurements on about 200 grains in different SEM micrographs. The microstructure of the alloys was characterized by means of transmission electron microscope (TEM, JEM-2000FX), and elemental analysis was accomplished by using an energy-dispersive X-ray spectroscopy (EDS, INCA) analytical system installed on TEM.

3 Results and discussion

The SEM or TEM micrographs of as-received tungsten, zirconium carbide powders and ball-milled W-ZrC powders are presented in Fig. 1. From the SEM micrograph of the as-received tungsten powders shown in Fig. 1(a) it can be seen that the tungsten particles have an average particle size of 400-600 nm and exhibit some aggregation. The particle size of ZrC is about 20-50 nm, as shown in Fig. 1(b). After ball-milling, ZrC particles were dispersed in W powders, and the aggregation of tungsten powders was well alleviated, as shown in Fig. 1(c).

Density and relative density of the SPSed W-ZrC materials are listed in Table 2. As can be seen, the relative density of all samples is higher than 97.5%. The SEM micrographs of the fracture surface (at room temperature) of W-ZrC materials are shown in Fig. 2, where the fracture surface of pure tungsten adopted from Ref. [19] was also shown for comparison. It can be seen that in all samples very few pores were found, implying the high relative density.

Table 1. Chemical composition of the as-received tungsten powders (wt.%)

	Cr	Ti	Fe	O	C	P	S	N	W
W powder	0.0005	0.0005	0.001	0.24	0.0029	0.0005	0.0005	-	Bal

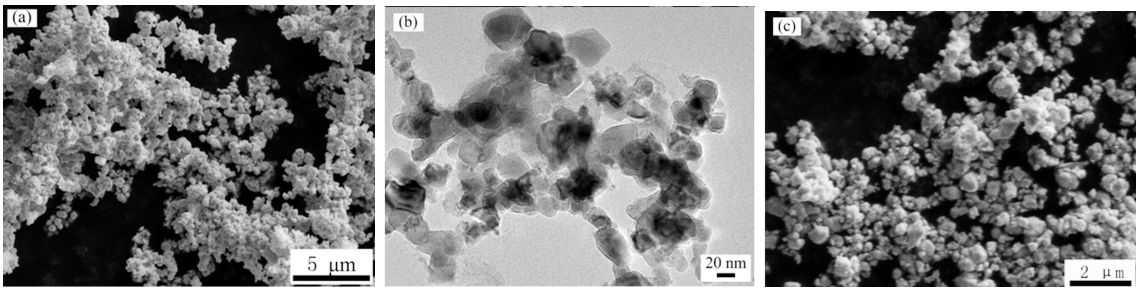

Fig.1 (a) SEM images of as-received tungsten powders, (b) TEM images of raw zirconium carbide powders and (c) SEM images of ball-milled W-ZrC powders

Table 2. Density, grain size and Vickers micro-hardness of spark plasma sintered pure W and W-ZrC alloys

Materials	Density (g/cm^3)	Relative density (%)	Grain size (μm)	Hv 100 g (GPa)
W [a]	18.8±0.06	97.4±0.31	4.1	4.51±0.14
W-0.2wt%ZrC	18.7±0.06	97.5±0.31	4.1	5.02±0.08
W-0.5wt%ZrC	18.6±0.06	97.5±0.31	4.2	5.07±0.08
W-1.0wt%ZrC	18.5±0.07	97.9±0.37	2.7	5.73±0.09

[a] [19]

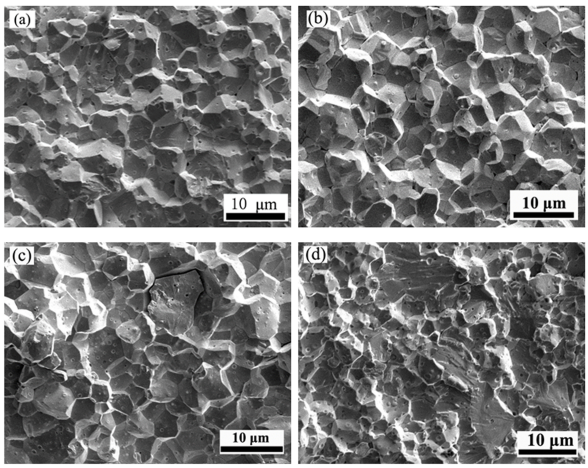

Fig.2 SEM micrographs of tensile fracture surface for (a) pure W [19], (b) W-0.2wt% ZrC, (c) W-0.5wt% ZrC and (d) W-1.0wt% ZrC

By assuming spherical grains, the diameters of about 200 tungsten grains from the SEM images were measured in each sample, and the average grain size of tungsten containing a different amount of ZrC is calculated and listed in Table 2, where the results of pure tungsten [19] are also shown for comparison. The grain size distribution of pure tungsten, W-0.2wt% ZrC and W-0.5wt% ZrC is in the range of 3-6 μm and the average grain size is about 4.1 μm. For the W-1.0wt% ZrC, however, much finer grains were obtained and the average size was only 2.7 μm. This indicated that 1.0wt% ZrC addition could effectively inhibit the grain growth during the sintering process.

Vickers micro-hardness of W-(0.2, 0.5, 1.0)wt% ZrC materials are 5.02 GPa, 5.07 GPa and 5.73 GPa, respectively, as listed in Table 2. As the ZrC addition increased from 0.2wt% to 1.0wt%, the Vickers micro-hardness increased from 5.02 GPa to 5.73 GPa, which is much higher than the value of pure W (4.5 GPa). The increase of hardness may come partially from the dispersion strengthening of nano-sized zirconium carbide and partially from the refined grains of tungsten containing ZrC.

The engineering stress-strain curves of W-ZrC materials at various temperatures are presented in Fig. 3. The tensile strength deduced from the stress-strain curves and the total elongations determined by measuring the length of the fractured samples using a vernier caliper are listed in Table 3, where the results of pure W [20] are presented for comparison. For the spark plasma sintered pure W, the DBTT was estimated in the range of 600 °C-700 °C. However, the W-(0.2, 0.5, 1.0)wt% ZrC materials exhibit obvious ductility at 600 °C and typical brittle fracture at 500 °C, suggesting a DBTT in the range of 500 °C-600 °C which is about 100 °C lower than that of pure W.

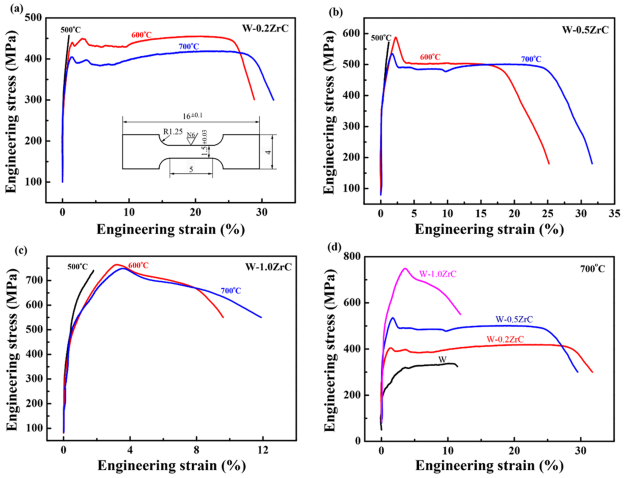

Fig.3 Tensile behaviors for (a) W-0.2wt% ZrC, (b) W-0.5wt% ZrC, (c) W-1.0wt% ZrC at various temperatures and (d) tensile curves of pure W [20] and W-(0.2, 0.5, 1.0)wt% ZrC at 700 °C

It can be seen from Fig. 3(a)-(c) and Table 3 that the high-temperature strength of the W containing ZrC is much higher than that of pure W at a comparative temperature. For a more detailed comparison, the stress-strain curves at 700 °C of the pure W and W-(0.2, 0.5, 1.0)wt% ZrC samples are plotted together in Fig. 3(d).

Table 3. Tensile properties of W alloys at various temperatures

Alloys	Tensile strength (MPa)/ elongation (%)		
	500 °C	600 °C	700 °C
W[b]	-	211[c]/-	337/11.6±0.4
W-0.2ZrC	457±35[c] /-	455±13/27.6±0.4	419±16/30.0±0.4
W-0.5ZrC	572±22[c] /-	588±8/17.6±0.4	535±15/24.8±0.4
W-1.0ZrC	741±30[c] /-	764±12/8.4±0.4	749±18/10.4±0.4

[b] [20], [c] brittle fracture

At 700 °C, the tensile strengths of pure W and W-(0.2, 0.5, 1.0) wt% ZrC materials are 337 MPa, 419 MPa, 535 MPa and 749 MPa, respectively, as listed in Table 3, indicating that the tensile strength increases with increasing ZrC addition from 0.2wt% to 1.0wt%. It is worth noting that the tensile strength of W-1.0wt% ZrC samples at 700 °C (749 MPa) is 122% higher than that of pure W (337 MPa). This value is even higher than that of hot rolled W-Zr-C, W-Ta-C, and W-Nb-C at 500 °C [21], which is in the range of 400-600 MPa.

The ductility could also be improved by adding a small amount of zirconium carbide. As shown in Fig. 3 and listed in Table 3, the elongation values of W-(0.2, 0.5, 1.0)wt% ZrC at 600 °C are 27.6%, 17.6% and 8.4%, respectively, while pure W is brittle at 600 °C. At 700 °C, the elongation values of W-(0.2, 0.5, 1.0)wt% ZrC are 30.4%, 24.8% and 10.4%, respectively, all of which are higher than or comparable to the value of pure W (11.6%). The W-0.2wt% ZrC sample exhibits the highest elongation and more ZrC addition would decrease the elongation value.

The mechanism for high strength and ductility of the W-ZrC alloys was analyzed based on microstructure characterization. In order to characterize the dispersion of the nano-size particles, TEM analysis was conducted. Particles with a size of 20-200 nm were found in W-0.2wt% ZrC and W-0.5wt% ZrC alloys respectively. Most particles are nano-sized and homogeneously dispersed in the tungsten grain interior, while few particles are found on the tungsten GBs and their average size (more than 100 nm) is relatively larger than those in the tungsten grain interior. A similar particles distribution was found in W-1.0wt% ZrC sample and not shown here.

To further clarify the phase of such particles, selected area electron diffraction (SAED) and EDS were employed. Particles bounding to the GBs in W-0.2wt% ZrC were analyzed in detail, as indicated by an arrow in Fig. 4(a), and the corresponding SAED pattern is depicted in the inset. The SAED results reveal that this particle is crystalline with a cubic structure. In Fig. 4(b), the EDS analysis of this particle shows that W, Zr, C and O signals were detected and the approximate atomic ratio is 1:14:26:59. More particles which bound to or near the GBs were investigated through EDS analysis, and oxygen was always detected in these particles. Combined with the above SAED analysis, it is reasonable to suggest that particles bound to or near the GBs are Zr-C-O phase with cubic structure [22]. The existence of oxygen in the particles bound to or near the GBs can be further confirmed from the lattice parameter of the cubic structure (0.474 nm), as calculated from the SAED, which is slightly larger than that of the ZrC phase (0.468 nm). The formation of the Zr-C-O particles was most probably owing to the ZrC particles capturing the trace impurity oxygen in tungsten during the sintering process.

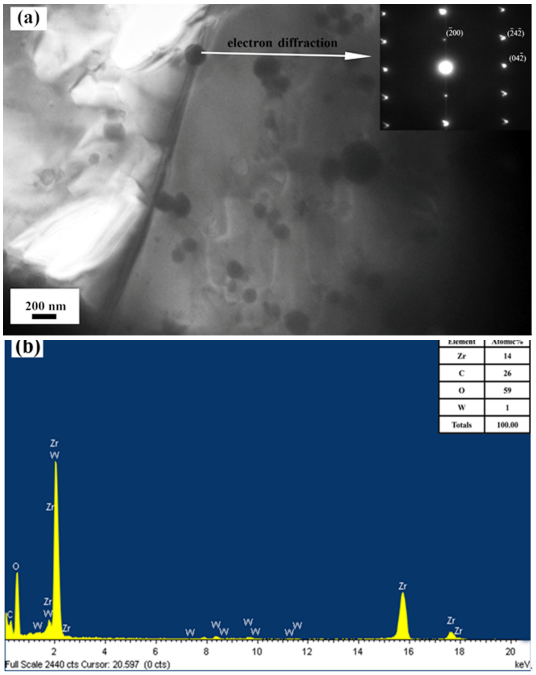

Fig.4 SAED pattern and EDS spectra of the nano-sized particle bounding to the GBs of tungsten in W-0.2wt% ZrC, (a) TEM image of particles distribution and SAED pattern (inset) and (b) EDS spectra and atomic ratio (inset)

Particles dispersed in the tungsten grain interior, as shown in Fig. 5(a), were analyzed as well. The SAED results reveal that the particle is crystalline with a cubic structure. The EDS analysis of the particles in the grain interior showed that only W, Zr and C signals were detected and the corresponding atomic ratio is 2:51:47, while an oxygen signal was not detected, as shown in Fig. 5(b). More particles were analyzed and the results suggest that the nano-size particles in the tungsten grain interior are the cubic ZrC phase.

Fig. 6 shows the TEM and HRTEM images of particles in the tungsten grain interior and on (or near) the GBs in W-0.5 wt%ZrC. A small spherical particle (about 30 nm) in the tungsten grain interior is indicated in Fig. 6(a) and the corresponding HRTEM image is shown in the inset. The measured spacings of three different crystalline faces are 0.231 nm, 0.273 nm

and 0.162 nm, which matched well to the values of the crystalline faces of cubic ZrC (200), (111) and (220) from the Powder Diffraction File (PDF) card (reference code: 00-001-1050), respectively. This further indicates that these nano-size particles in the tungsten grain interior are cubic ZrC. A larger particle (about 120 nm) near GBs is indicated in Fig. 6(b) and the HRTEM image is shown in the inset. The measured spacings of two different crystalline faces are 0.513 nm and 0.368 nm, which are consistent with the values of monoclinic ZrO_2 (100) and (110) from the PDF card (reference code: 00-001-0750), respectively. This result further illustrated that the ZrC particles could react with the trace impurity oxygen in tungsten to form zirconium oxide during the sintering process.

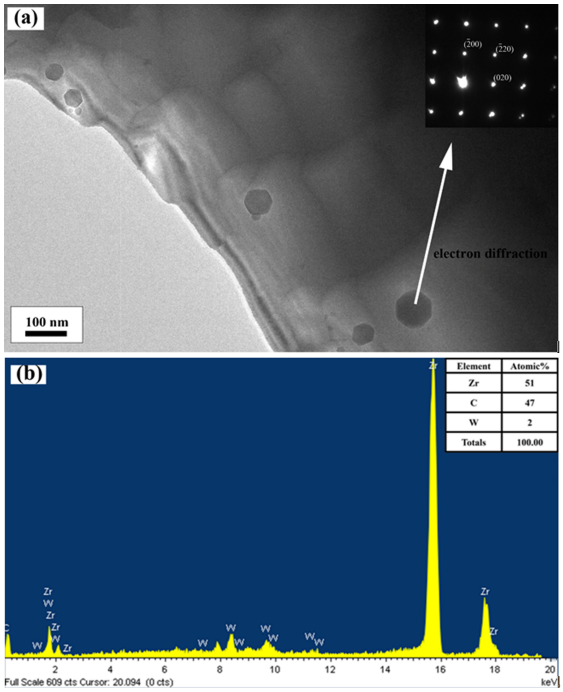

Fig.5 SAED pattern and EDS spectra of the nano-sized particle dispersing in the matrix of tungsten in W-0.2wt% ZrC, (a) TEM image of spherical particles and SAED pattern (inset) and (b) EDS spectra and atomic ratio (inset)

From the above analysis, the larger elongation, higher strength values and lower DBTT of W-0.2wt% ZrC and W-0.5wt% ZrC alloys can be reasonably understood as follows. The improved ductility can be attributed to the capture of trace impurity oxygen in tungsten by a small amount of zirconium carbide, while the high temperature strength was due to the pinning of dislocations and GBs by the dispersed ZrC, ZrO_2 and Zr-C-O nano-particles in the tungsten grain interior and on the GBs. Nevertheless, more ZrC addition drastically decreases the elongation though the strength may still increase, and as a result the W-1.0wt% ZrC exhibits a smaller elongation value (10.4%) than pure W (11.6%) at 700 °C. The reason may be that the excessive second phase particles at the GBs may also introduce stress concentrations and become possible sites of crack initiation [23], which would reduce the ductility.

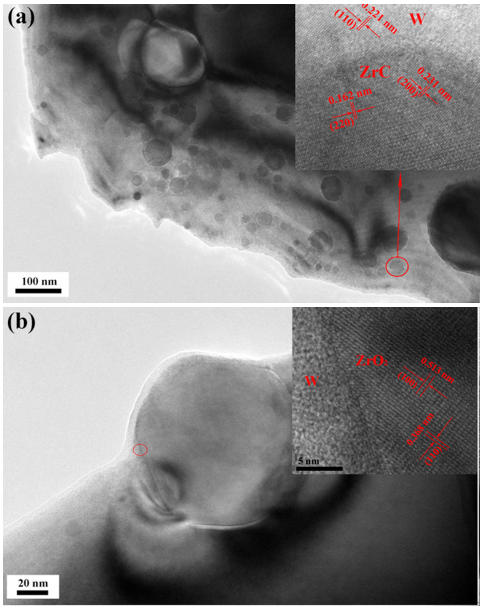

Fig.6 TEM images of W-0.5wt% ZrC composite, (a) TEM image of particles distribution in the grain interior and the HRTEM of the ZrC phase (inset) and (b) the ZrO_2 phase on the grain boundary (inset)

4 Conclusions

W-(0.2, 0.5, 1.0)wt% ZrC materials were fabricated by SPS method from the W and nano-size ZrC powders. The mechanical properties and microstructure were investigated. The results can be summarized as follows.

a. The relative density of all the samples was above 97.5%. The grain size of W-1.0wt% ZrC alloy is about 2.7 μm, which is much smaller than that of pure W, indicating that 1.0wt% ZrC addition could inhibit the grain growth during the sintering process. The DBTT of W-(0.2, 0.5, 1.0)wt% ZrC materials determined by a tensile test is in the range of 500 °C-600 °C, which is about 100 °C lower than that of pure W. Besides, the hardness at room temperature of the W-ZrC alloys is higher than that of pure W.

b. The addition of a small amount of ZrC could improve the ductility and high temperature strength of tungsten materials. However, too much ZrC addition (higher than 0.5%) would lead to the decrease of the elongation though the tensile strength still increased. The tungsten sample with 0.5wt% ZrC addition exhibits not only high tensile strength, but also improved ductility. The ultimate tensile strength and total elongation of W-0.5wt% ZrC alloy at 700 °C are 535 MPa and 24.8%, which are respectively 59% and 114% higher than those of pure W (337 MPa, 11.6%).

c. Microstructure analysis suggested that the nano-size ZrC particles located on the GBs of tungsten could capture the trace impurity oxygen in tungsten to form cubic Zr-C-O or the monoclinic ZrO_2 phase, which would reduce the influence of oxygen on grain boundary strength and thus enhance the ductility of tungsten based alloys. The nano-size ZrC dispersed in the tungsten grain interior and the Zr-C-O or ZrO_2 particles on

the GBs could pin down dislocations and GBs, and thus improve the high-temperature strength.

References

1 Norajitra P, Boccaccini L V, Diegele E, et al. 2004, J. Nucl. Mater., 329-333: 1594

2 Smid I, Pacher H D, Vieider G, et al. 1996, J. Nucl. Mater., 233-237: 701

3 Norajitra P, Boccaccini L V, Gervash A, et al. 2007, J. Nucl. Mater., 367-370: 1416

4 Kurishita H, Kobayashi S, Nakai K, et al. 2008, J. Nucl. Mater., 377: 34

5 Kurishita H, Amano K, Kobayashi S, et al. 2007, J. Nucl. Mater., 367-370: 1453

6 Funkenbusch A W, Bacon F and Lee D. 1979, Met. Trans. A., 10A: 1085

7 Joshi A and Stein D F. 1970, Met. Trans., 1: 2543

8 Liu J M and Shen B W. 1982, Acta Met., 30: 1197

9 Greger M, Cizek L and Widomska M. 2004, J. Mater. Process. Tech., 157: 683

10 Setyawan W and Kurtz R J. 2012, Scripta Mater., 66: 558

11 Kecskes L J, Cho K C, Dowding R J, et al. 2007, Mater. Sci. Eng. A: Struct., 467: 33

12 Liu R, Zhou Y, Hao T, et al. 2012, J. Nucl. Mater., 424: 171

13 Zhang T Q, Wang Y J, Zhou Y, et al. 2010, Mater. Sci. Eng. A, 527: 4021

14 Wesemann I, Spielmann W, Heel P, et al. 2010, Int. J. Refract. Met. Hard Mater., 28: 687

15 Kim Y, Hong M H, Lee S H, et al. 2006, Met. Mater. Int., 12: 245

16 Kurishita H, Kuwabara T, Hasegawa M, et al. 2005, J. Nucl. Mater., 343: 318

17 Samaras M, Derlet P M, Swygenhoven H V, et al. 2002, Phys. Rev. Lett., 88: 12

18 Shimada S. 1997, Solid State Ionics, 101-103: 749

19 Xie Z M, Liu R, Fang Q F, et al. 2014, J. Nucl. Mater., 444: 175

20 Liu R, Xie Z M, Hao T, et al. 2014, J. Nucl. Mater., 451: 35

21 Podyachev V N and Gavrilyuk M I. 1975, Metalloved. Term. Obrab. Met., 24-28

22 Preiss H, Berger L-M and Szulzewsky K. 1996, Carbon, 34: 109

23 Liu G, Zhang G J, Jiang F, et al. 2013, Nature Materials, 12: 344

(Manuscript received 25 November 2014)
(Manuscript accepted 18 March 2015)
E-mail address of corresponding author
FANG Qianfeng: qffang@issp.ac.cn